2.4 - Impacts of the Veer-Back Wind Profile on Observed Rotational Velocities in Supercell Thunderstorms

Nathan Wendt[a]

[a] *NOAA/National Weather Service/Storm Prediction Center, Norman, Oklahoma*

ABSTRACT: Within the operational severe storms forecasting community, the presence of the veer-back wind profile has been thought to have a detrimental effect on tornado potential. Previous work, while limited, has addressed some questions about the impacts of the veer-back wind profile on storm morphology and severity. Of particular note, numerical modeling has been used to try and quantify the impacts of backing aloft at various levels of the atmosphere. However, to date, little work on this topic has been done using observational data. Using storm reports, surface-modified RAP soundings, and rotational velocities from WSR-88D data, this work analyzes the impacts of veer-back wind profiles on observed supercell thunderstorms. Specifically, this work is focused on understanding both the magnitude and the layer of the atmosphere where backing winds with height have the most detrimental impact on significant tornado potential in supercell thunderstorms.

1. Introduction

There has been numerous studies on the impacts of vertical wind shear on the overall potential for and severity of supercell thunderstorms. More specifically related to this current study are those previous works that focused on various hodograph characteristics and their relationship with tornado potential (e.g., Markowski et al. 2003; Parker 2014; Coffer and Parker 2017; Coniglio and Parker 2020) and intensity (e.g., Esterheld and Giuliano 2008; Nowotarski and Jones 2018; Coffer et al. 2019, 2020).

One particular hodograph shape that has been at least anecdotally thought to have a negative impact on tornado potential is the veer-back profile. This refers to when the shear vector veers (turns clockwise) with height then begins to back (turn counter-clockwise) with height through some layer. Changes in wind speed, wind direction, or some combination of both can contribute to a hodograph taking on this sort of shape—a "kink" or "weakness" within the profile. Despite the suspected negative impacts of this wind profile, very little research has been done specifically on this topic. There have been case studies (Mulholland et al. 2015) and some modeling work as well (Warren et al. 2017). The most comprehensive work on the veer-back wind profile was done by Parker (2017). That study did several simulations wherein the location and magnitude of the backing aloft was varied in the vertical. Results showed that modeled supercell intensity and longevity were not significantly impacted by the presence of backing aloft except where:

1. SRH was lowered due to the changes in storm motion
2. Dynamical accelerations were less favorable
3. Downshear precipitation distribution impacted storm inflow negatively

Other examples in the literature show that backing aloft can occur in cases where storms were nontornadic (Parker 2014) as well as cases where significantly tornadic storms occurred in the presence of backing aloft (Orf et al. 2017; Nowotarski and Jensen 2013).

What is not present within the current body of literature is an investigation of the impacts of the veer-back wind profile using observational data (at least to the greatest extent possible). This work intends to help fill that gap. Another area of interest for this study will be to assess whether backing aloft occurs within the effective inflow layer of storms. The effective inflow layer has been shown to be important in discriminating between significantly tornadic and nontornadic environments (Thompson et al. 2007). That said, the primary two questions this work seeks to answer are:

- Is backing aloft occurring within the inflow layer important?
- Where in the inflow layer does backing aloft have the most impact?

2. Data

In order to properly relate storm environments to a particular storm mode, the Storm Prediction Center (SPC) convective mode and rotational velocity database was used (Smith et al. 2012). Storm modes and their WSR-88D-derived rotational velocities were manually retrieved and documented using objective criteria described in Smith et al. 2012. Additionally, near-storm environment data was also investigated and attached to each severe weather event (Thompson et al. 2012). These data are available for

Corresponding author: Nathan Wendt, nathan.wendt@noaa.gov

tornadoes, with a smaller subset of data also available for severe wind and hail.

Environmental data used in this work comes from the SPC mesoscale surface objective analysis (SFCOA). SFCOA is based on the 13 km RAP model (Benjamin 2016; Hu et al. 2017). For the lowest model level, 2-m temperature and humidity as well as 10-m winds were replaced by a two-pass Barnes analysis of current surface observations (Bothwell et al. 2002). Lastly, the near-surface-modified model data is post-processed to a 40-km grid with vertical levels every 25 mb.

Though data is available beginning in 2003, this analysis will use data from 2009–2021. Beginning in 2009 is practical due to the availability of super-resolution data from the WSR-88D network (Torres and Curtis 2007). This is also consistent with previous work (Smith et al. 2012, 2015, 2020).

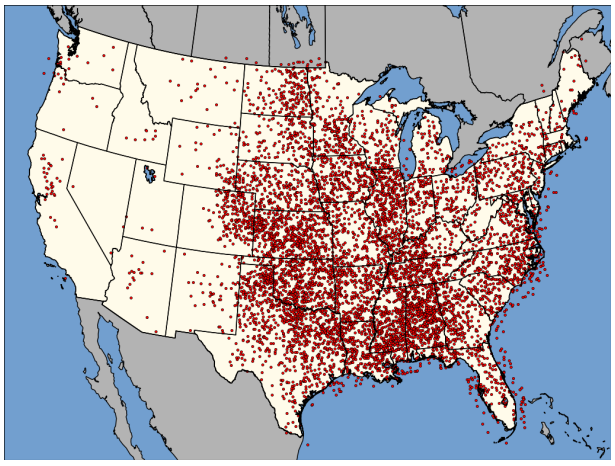

FIG. 1. Locations of matched soundings.

3. Methods

a. Sounding matching

The SPC convective mode and rotational velocity dataset contains data for each tornado report/track (i.e., there is rotational velocity and associated environmental data along the track of any tornado as it crossed analysis hours and grid boxes within the SFCOA 40-km grid). Rotational velocities used were only from scans with beam heights at or below 10000 ft above radar level (ARL). These data (through the 2009–2021 period) were the starting point for the analysis. Only right-moving supercell storm mode events were considered. This was done to restrict wind profiles to a consistent subset; more disorganized or linear storm modes can occur within a broader range of wind profiles, making interpretation of results more difficult. Given the location of events within the database, SFCOA soundings were then matched to each event—one from the actual grid point along with the eight surrounding grid points. Where any additional calculations of environmental fields were needed, SHARPlib (Halbert et al. 2022) was used. This library is consistent with the calculations done for the actual SFCOA grids.

b. Sounding QC

After soundings were matched, some quality control needed to be done to reduce the potential for convectively contaminated profiles to influence the results. First, model vertical motion was used to filter soundings with values larger than typical synoptic scale motions as follows

$$|\omega| \geq 0.01\ Pa\ s^{-1} \tag{1}$$

Soundings with negative effective SRH values were also removed as these were not likely to be representative inflow soundings. Then, from the remaining soundings, the sounding with the largest MUCAPE and least MUCIN was chosen as the representative sounding for that particular event. All valid soundings were then standardized to 100 m vertical resolution up to 12 km. In total, 7878 wind profiles remained after the QC and filtering process. The spatial distribution of all matched soundings is shown in Figure 1. Even with the filtering, some convective contamination is still possible.

c. Other definitions

Where reference is made to significant (EF2+) tornadoes in this work, this is referring to rotational velocities (V_{rot}) of $\geq$ 60 kts. This is a reasonable threshold as the conditional probability of an EF2/EF3 tornado given $V_{rot} \geq 60\ kts$ was calculated to be 50% by Smith et al. (2015).

To quantify the changes in the wind profile, each vertical profile was examined for the magnitude of difference in the speed and direction between each layer. These values were then summed within a layer, the effective inflow layer in this case, to come up with a representative value. When referring to speed increases or speed decreases within a layer, it means the total magnitude of speed increase or decrease, respectively. For veering and backing between layers, it is similarly the total veering and total backing within that layer.

4. Results

a. Overview

Figure 2 shows where in the vertical wind profile changes in speed (left histogram) and direction (right histogram) occur. There is a local maxima in speed decrease between 800–750 hPa layer. This same layer also coincides with a steady increase in the frequency of backing winds. Also included in Figure 2 is the frequency of where effective

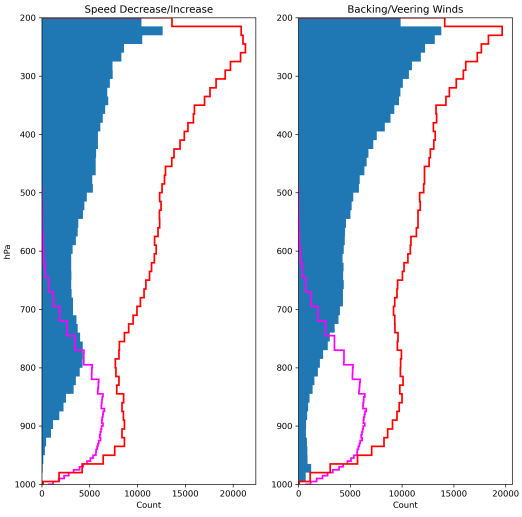

FIG. 2. Frequency of changes in speed (left) and direction (right) with height (hPa) where increases/veering is the red line, decreasing/backing is the blue fill. The magenta line is the frequency of where effective inflow layers occurred.

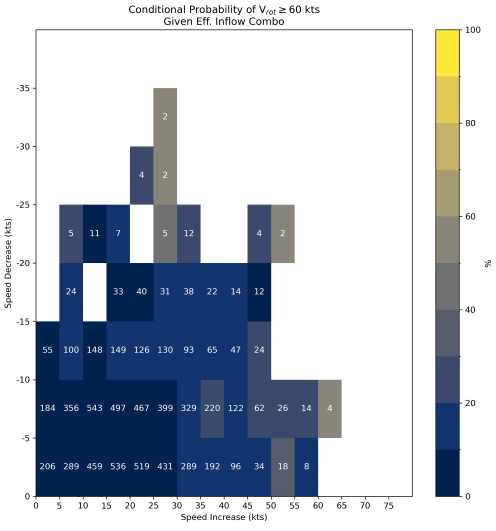

FIG. 3. Conditional probability of $V_{rot} \geq 60\ kts$ given a combination of speed increase and speed decrease within the effective inflow layer.

inflow layers occurred within the vertical profile (magenta line). Portions of the inflow layers are impacted by both speed decreases and backing winds, particularly the upper and middle sections.

b. Changes in speed

Figure 3 shows the probability of a significant tornado given a combination of speed increase and speed decrease within the effective inflow layer. The dominant signal within this figure is that greater amounts of speed increase (i.e., greater positive shear) in the inflow layer givens a greater conditional likelihood of a significant tornado. As speed decrease magnitudes get larger, there is a general signal that there is a decrease in significant tornado potential. However, if the speed increase magnitude is larger enough, there is some amount of tolerance to a larger speed decrease magnitude as evidenced by the similar conditional probabilities. There are some higher conditional probabilities where low speed increase magnitudes occur with high speed decrease magnitudes, though the sample sizes are small. It is not clear why this occurs and would require further investigation into the wind profiles associated with these events.

c. Changes in direction

Figure 4 shows the probability of a significant tornado given a combination of total veering and total veering within the effective inflow layer. There is a modest signal for stronger veering to increase the conditional probability of a significant tornado. That signal is not uniform, however. The signal for larger magnitudes of backing having a negative impact on significant tornado potential is weaker. Given the amount of clustering of total backing $\leq -20\ kts$ it is difficult to say whether larger backing magnitudes can be tolerated with larger veering magnitudes.

d. Inflow layer

Figure 5 shows the conditional probability of a significant tornado given a speed decrease magnitude in the effective inflow layer. Here, the inflow layer has been split into thirds to try and ascertain whether there is a portion of the inflow layer that is impacted more by the presence of backing aloft. The upper third is in red, the middle third in blue, and the lower third in green. The sample size for this analysis is rather small, in particular for the lower third of the inflow layer and with the largest speed decrease magnitudes. However, the weak signal that does exits suggests that there is a greater impact when weaknesses in the wind profile occur in the lower portions of the effective inflow layer.

5. Discussion

Backing aloft, while it can occur at upper levels, shows some tendency to occur in portions of the low to mid levels (Figure 2). When occurring at the lower portions of the troposphere, there is greater potential for it to occur within

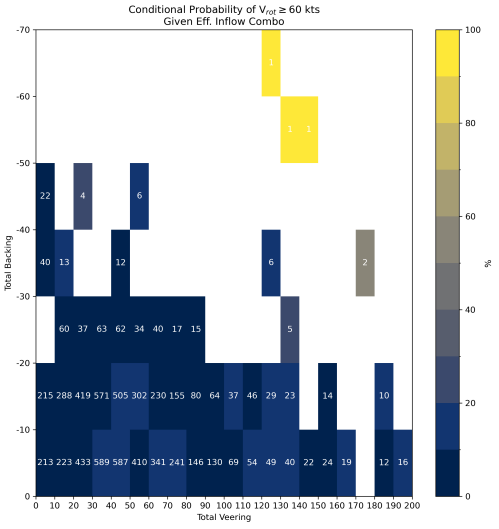

FIG. 4. Conditional probability of $V_{rot} \geq 60\ kts$ given a combination of total veering and total backing within the effective inflow layer.

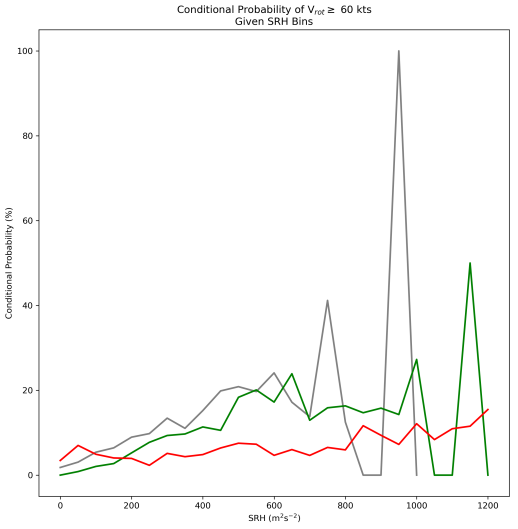

FIG. 6. Conditional probability of $V_{rot} \geq 60\ kts$ given effective SRH (red), 0–3 km SRH (green), and 0–1 km SRH (gray).

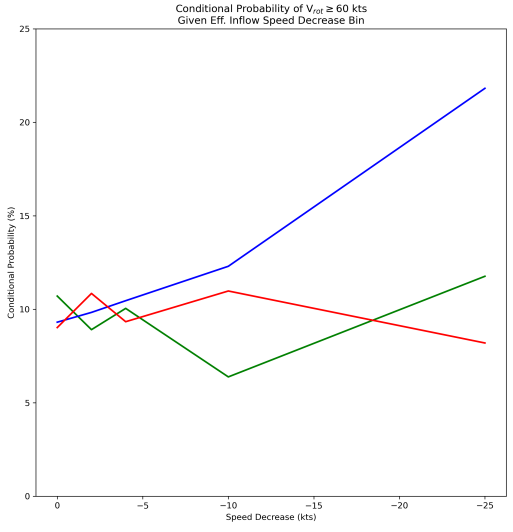

FIG. 5. Conditional probability of $V_{rot} \geq 60\ kts$ given a speed decrease magnitude in the effective inflow layer zone. The zones are as follows: upper third (red), middle third (blue), and lower third (green).

the effective inflow layer. Based on the results of this study, both backing and decreases in speed of the winds within the effective inflow layer reduce the potential for significant tornadoes (Figures 3 and 4). However, when veering and increases in speed of the winds in the inflow layer are strong enough, the backing/decrease tends to have a lesser impact. This would suggest that there are cases in which a marginal significant tornado environment could become unsupportive due to these unfavorable layers of backing. This study also showed at least weak evidence for backing within the lower portions of the inflow layer to be the most impactful in terms of reducing significant tornado potential (Figure 5). This results makes physical sense and is consistent to what was found in Coffer et al. (2020).

The argument that how backing aloft impacts SRH is more important than the mere existence of backing aloft, which was suggested by Parker (2017), seems to be the most relevant factor to forecasting. When applying the same conditional probability analysis to SRH fields (Figure 6), there is a clear signal that larger SRH values support higher conditional probability of a significant tornado. SRH does a more elegant job of explaining what is going on physically and offers more value when trying to forecast significant tornadoes and severe weather in general.

What this study does not do is get at the mechanisms that bring about backing aloft within the larger-scale atmospheric pattern. As Parker (2017) suggests, investigating these patterns may offer greater insight and allow forecasters to more readily anticipate when and where in the profile backing aloft could occur.

Data availability statement. Convective mode, rotational velocity, and SFCOA data are all available upon request.

References

Benjamin, S. G., 2016: A north american hourly assimilation and model forecast cycle: The rapid refresh. *Mon. Wea. Rev.*, **144**, 1669–1694, https://doi.org/10.1175/MWR-D-15-0242.1.

Bothwell, P., J. Hart, and R. Thompson, 2002: An integrated three-dimensional objective analysis scheme in use at the Storm Prediction Center. *21st Conf. on Severe Local Storms*, Amer. Meteor. Soc., San Antonio, TX, JP3.1, URL https://ams.confex.com/ams/pdfpapers/47482.pdf.

Coffer, B. E., and M. D. Parker, 2017: Simulated supercells in nontornadic and tornadic vortex2 environments. *Mon. Wea. Rev.*, **145 (1)**, 149 – 180, https://doi.org/10.1175/MWR-D-16-0226.1.

Coffer, B. E., M. D. Parker, R. L. Thompson, B. T. Smith, and R. E. Jewell, 2019: Using near-ground storm relative helicity in supercell tornado forecasting. *Wea. Forecasting*, **34 (5)**, 1417 – 1435, https://doi.org/10.1175/WAF-D-19-0115.1.

Coffer, B. E., M. Taszarek, and M. D. Parker, 2020: Near-ground wind profiles of tornadic and nontornadic environments in the united states and europe from era5 reanalyses. *Wea. Forecasting*, **35 (6)**, 2621 – 2638, https://doi.org/10.1175/WAF-D-20-0153.1.

Coniglio, M. C., and M. D. Parker, 2020: Insights into supercells and their environments from three decades of targeted radiosonde observations. *Mon. Wea. Rev.*, **148 (12)**, 4893 – 4915, https://doi.org/10.1175/MWR-D-20-0105.1.

Esterheld, J. M., and D. J. Giuliano, 2008: Discriminating between tornadic and non-tornadic supercells: A new hodograph technique. *Electron. J. Severe Storms Meteor.*, **3 (2)**, https://doi.org/10.55599/ejssm.v3i2.15.

Halbert, K., J. Hart, and R. Thompson, 2022: SHARPlib v0.0.1. URL https://github.com/keltonhalbert/SHARPlib.

Hu, M., S. G. Benjamin, T. T. Ladwig, D. C. Dowell, S. S. Weygandt, C. R. Alexander, and J. S. Whitaker, 2017: Gsi three-dimensional ensemble–variational hybrid data assimilation using a global ensemble for the regional rapid refresh model. *Mon. Wea. Rev.*, **145**, 4205–4225, https://doi.org/10.1175/MWR-D-16-0418.1.

Markowski, P., C. Hannon, J. Frame, E. Lancaster, A. Pietrycha, R. Edwards, and R. L. Thompson, 2003: Characteristics of vertical wind profiles near supercells obtained from the rapid update cycle. *Wea. Forecasting*, **18 (6)**, 1262 – 1272, https://doi.org/10.1175/1520-0434(2003)018⟨1262:COVWPN⟩2.0.CO;2.

Mulholland, J., J. W. Frame, and S. M. Steiger, 2015: A numerical investigation into the presence of veer-back-veer vertical wind profiles in supercell environments: A case study of 30 and 31 may 2013. *16th Conf. on Mesoscale Processes*, Amer. Meteor. Soc., Boston, MA, 3.7, URL https://ams.confex.com/ams/16Meso/webprogram/Paper274591.html.

Nowotarski, C. J., and A. A. Jensen, 2013: Classifying proximity soundings with self-organizing maps toward improving supercell and tornado forecasting. *Wea. Forecasting*, **28 (3)**, 783 – 801, https://doi.org/10.1175/WAF-D-12-00125.1.

Nowotarski, C. J., and E. A. Jones, 2018: Multivariate self-organizing map approach to classifying supercell tornado environments using near-storm, low-level wind and thermodynamic profiles. *Wea. Forecasting*, **33 (3)**, 661 – 670, https://doi.org/10.1175/WAF-D-17-0189.1.

Orf, L., R. Wilhelmson, B. Lee, C. Finley, and A. Houston, 2017: Evolution of a long-track violent tornado within a simulated supercell. *Bull. Amer. Meteor. Soc.*, **98 (1)**, 45 – 68, https://doi.org/10.1175/BAMS-D-15-00073.1.

Parker, M. D., 2014: Composite vortex2 supercell environments from near-storm soundings. *Mon. Wea. Rev.*, **142 (2)**, 508 – 529, https://doi.org/10.1175/MWR-D-13-00167.1.

Parker, M. D., 2017: How much does "backing aloft" actually impact a supercell? *Wea. Forecasting*, **32 (5)**, 1937 – 1957, https://doi.org/10.1175/WAF-D-17-0064.1.

Smith, B. T., R. L. Thompson, A. R. Dean, and P. T. Marsh, 2015: Diagnosing the conditional probability of tornado damage rating using environmental and radar attributes. *Wea. Forecasting*, **30 (4)**, 914 – 932, https://doi.org/10.1175/WAF-D-14-00122.1.

Smith, B. T., R. L. Thompson, J. S. Grams, C. Broyles, and H. E. Brooks, 2012: Convective modes for significant severe thunderstorms in the contiguous united states. part i: Storm classification and climatology. *Wea. Forecasting*, **27 (5)**, 1114 – 1135, https://doi.org/10.1175/WAF-D-11-00115.1.

Smith, B. T., R. L. Thompson, D. A. Speheger, A. R. Dean, C. D. Karstens, and A. K. Anderson-Frey, 2020: Wsr-88d tornado intensity estimates. part i: Real-time probabilities of peak tornado wind speeds. *Wea. Forecasting*, **35 (6)**, 2479 – 2492, https://doi.org/10.1175/WAF-D-20-0010.1.

Thompson, R. L., C. M. Mead, and R. Edwards, 2007: Effective storm-relative helicity and bulk shear in supercell thunderstorm environments. *Wea. Forecasting*, **22 (1)**, 102 – 115, https://doi.org/10.1175/WAF969.1.

Thompson, R. L., B. T. Smith, J. S. Grams, A. R. Dean, and C. Broyles, 2012: Convective modes for significant severe thunderstorms in the contiguous united states. part ii: Supercell and qlcs tornado environments. *Wea. Forecasting*, **27 (5)**, 1136 – 1154, https://doi.org/10.1175/WAF-D-11-00116.1.

Torres, S. M., and C. D. Curtis, 2007: Initial implementation of super-resolution data on the nexrad network. preprints, 23rd int. conf. on interactive information processing systems. *23rd Int. Conf. on Interactive Information Processing Systems*, Amer. Meteor. Soc., San Antonio, TX, 5B.10, URL https://ams.confex.com/ams/pdfpapers/116240.pdf.

Warren, R. A., H. Richter, H. A. Ramsay, S. T. Siems, and M. J. Manton, 2017: Impact of variations in upper-level shear on simulated supercells. *Mon. Wea. Rev.*, **145 (7)**, 2659 – 2681, https://doi.org/10.1175/MWR-D-16-0412.1.